ARTICLE

doi:10.1038/nature17157

Deletions linked to *TP53* loss drive cancer through p53-independent mechanisms

Yu Liu[1,2]*, Chong Chen[1,2]*, Zhengmin Xu[1], Claudio Scuoppo[3], Cory D. Rillahan[2], Jianjiong Gao[4], Barbara Spitzer[5,6], Benedikt Bosbach[2], Edward R. Kastenhuber[2], Timour Baslan[2], Sarah Ackermann[2], Lihua Cheng[7], Qingguo Wang[4], Ting Niu[7], Nikolaus Schultz[4], Ross L. Levine[6], Alea A. Mills[8] & Scott W. Lowe[2,9]

Mutations disabling the *TP53* tumour suppressor gene represent the most frequent events in human cancer and typically occur through a two-hit mechanism involving a missense mutation in one allele and a 'loss of heterozygosity' deletion encompassing the other. While *TP53* missense mutations can also contribute gain-of-function activities that impact tumour progression, it remains unclear whether the deletion event, which frequently includes many genes, impacts tumorigenesis beyond *TP53* loss alone. Here we show that somatic heterozygous deletion of mouse chromosome 11B3, a 4-megabase region syntenic to human 17p13.1, produces a greater effect on lymphoma and leukaemia development than *Trp53* deletion. Mechanistically, the effect of 11B3 loss on tumorigenesis involves co-deleted genes such as *Eif5a* and *Alox15b* (also known as *Alox8*), the suppression of which cooperates with *Trp53* loss to produce more aggressive disease. Our results imply that the selective advantage produced by human chromosome 17p deletion reflects the combined impact of *TP53* loss and the reduced dosage of linked tumour suppressor genes.

Cancer arises through the acquisition of genetic and epigenetic changes that drive tumorigenesis. While most efforts to understand the origins of these entities have focused on the identification and functional characterization of somatic single nucleotide variants (SNVs) that activate oncogenes or inactivate tumour suppressors, the vast majority of human cancers also harbour large copy number variants (CNVs) that impact gene dosage through gain or loss of whole chromosomes or chromosome segments[1]. For example, recurrent segmental deletions—such as those affecting chromosome 17p—are extremely common in human cancers yet are widely considered to arise because of selection for a single 'driver' in the deleted region, with the adjacent gene losses reflecting 'passenger' events that have no effect on tumour phenotypes. However, evidence is emerging from short hairpin RNA (shRNA) screens and bioinformatic approaches that these lesions may target more than one relevant activity[2–5]. If true, then the impact of segmental deletions on tumour development would be fundamentally distinct from SNVs, yet, given their frequent occurrence, disproportionately understudied.

Chromosome 17p configurations in human cancer

We decided to study 17p deletion as a prototype of a recurrent cancer-associated deletion owing to its high frequency and invariable inclusion of *TP53*, an extensively studied tumour suppressor gene that is considered to be the major driver of 17p loss[6,7]. To characterize better the nature and scope of these deletions, we analysed genomic data from 4,994 tumours across 18 cancer types (http://www.cbioportal.org; accessed 29 October 2014). This survey confirmed previous indications that mutation and/or deletion of the *TP53* tumour suppressor gene occurs in approximately ~50% of all human cancers[8]. We then classified 17p-altered tumours as to whether they displayed *TP53* mutation (encompassing missense, nonsense and frameshift mutations), deletion (as defined by a reduction in *TP53* copy number), or both (Fig. 1a). The most common *TP53* configuration involves a missense mutation together with a segmental 17p deletion, although a substantial fraction of p53-altered tumours harboured chromosome 17p deletion together with an apparently wild-type *TP53* allele. Similar results were observed in blood cancers, in which *TP53* mutations and/or 17p loss are less common but are linked to a particularly dismal prognosis[9,10]. Hence, the frequency of 17p deletion may even exceed point mutations within the *TP53* gene.

Chromosome 17p deletions frequently encompass all or most of the chromosome arm (Fig. 1b). In addition to *TP53*, this region encodes over 300 protein-coding genes that include other established or putative tumour suppressors[11–13]. Unexpectedly, *TP53* was not identified as a candidate tumour suppressor in non-Hodgkin lymphoma or acute myeloid leukaemia (AML) using GISTIC, an algorithm designed to pinpoint candidate drivers from CNV data by identifying 'epicentres' of gain or loss[14] (Fig. 1b and Extended Data Fig. 1b). Moreover, AMLs harbouring a *TP53* mutation together with a 17p deletion displayed a worse prognosis than those harbouring *TP53* mutations alone (Fig. 1c and Extended Data Fig. 1c). Collectively, these data raise the possibility that additional genes drive selection for 17p loss during tumorigenesis.

Modelling 17p13 deletions in the mouse

We decided to test this hypothesis in mice. To produce a strain capable of modelling somatic 17p deletions, we used the MICER chromosome engineering strategy developed previously[15] to introduce *loxP* sites and a split *HPRT* gene into chromosomal regions flanking the *Alox12* and *Sco1* genes on mouse chromosome 11B3, which is a 4 Mb region on mouse chromosome 11 that is syntenic to human 17p13.1 (Fig. 2a, b and Extended Data Fig. 2a, b). Candidate clones were treated with adenovirus (Adeno)-*cre* to recombine the 11B3 region, selected in

[1]Department of Hematology and Department of Liver Surgery, State Key Laboratory of Biotherapy and Cancer Center, West China Hospital, Sichuan University and National Collaborative Innovation Center, Chengdu 610041, China. [2]Department of Cancer Biology and Genetics, Memorial Sloan Kettering Cancer Center, New York, New York 10065, USA. [3]Institute for Cancer Genetics, Columbia University Medical Center, New York, New York 10032, USA. [4]Kravis Center for Molecular Oncology, Memorial Sloan Kettering Cancer Center, New York, New York 10065, USA. [5]Department of Pediatrics, Memorial Sloan Kettering Cancer Center, New York, New York 10065, USA. [6]Human Oncology & Pathogenesis Program and Leukemia Service, Memorial Sloan Kettering Cancer Center, New York, New York 10065, USA. [7]Department of Hematology & Research Laboratory of Hematology, West China Hospital, Sichuan University, Chengdu 610041, China. [8]Cold Spring Harbor Laboratory, Cold Spring Harbor, New York 11724, USA. [9]Howard Hughes Medical Institute, New York, New York 10065, USA.
*These authors contributed equally to this work.

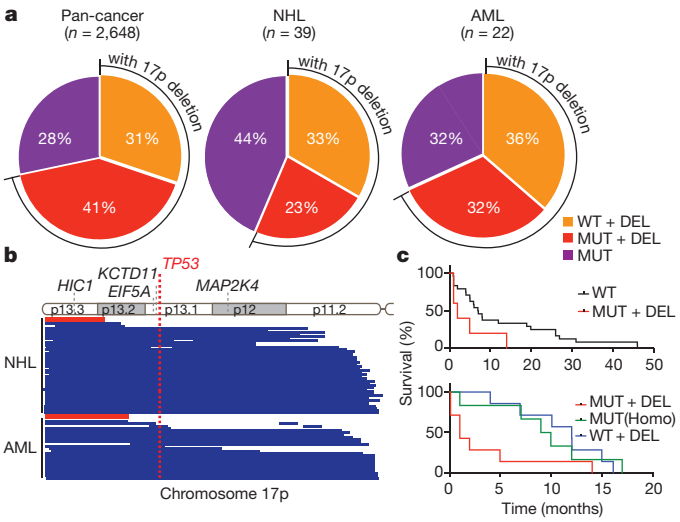

Figure 1 | The frequency, scope, and prognostic value of chromosome 17p alterations in human cancers. a, The nature of *TP53*-containing chromosome 17p alterations in pan-human cancer (left), non-Hodgkin lymphomas (NHL; middle) and AML (right). DEL, deletion; MUT, mutations; WT, wild-type. **b**, The extent of chromosome 17p deletions in NHL (44 cases; top) and AML (25 cases; bottom) data sets, irrespective of *TP53* deletion, as determined by single nucleotide polymorphism (SNP) array analysis. Each line represents one patient. Red bar indicates the significant copy number loss ($q < 0.25$) analysed by GISTIC algorithm. **c**, Overall survival of complex-karyotype AML patients containing both 17p deletion and *TP53* mutation as compared to those without any *TP53* alteration (top; $P = 0.076$), those with homozygous (Homo) *TP53* point mutations (bottom; $P = 0.059$), or those with 17p deletion without any detectable *TP53* mutation (bottom; $P = 0.03$). All are log-rank test.

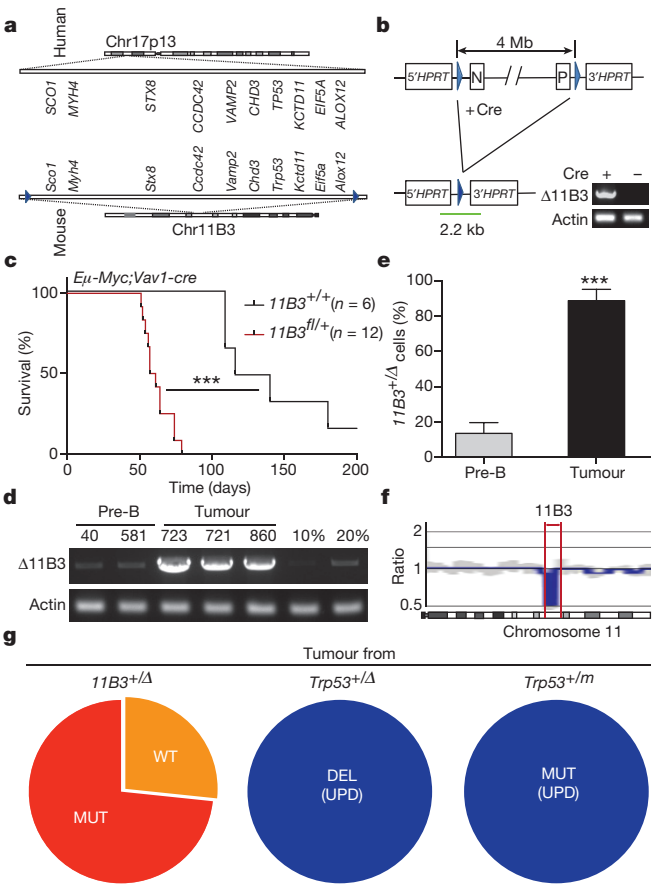

Figure 2 | A mouse model of human 17p13.1 deletion accelerates lymphoma development. a, The synteny of human chromosome (Chr) 17p13.1 and mouse chromosome 11B3 (from *Sco1* to *Alox12b*, ~4 Mb), with several representative genes listed. Blue arrowheads denote *loxP* sites. **b**, Conditional, 11B3-deletion strategy with PCR analysis (corresponding to the green bar) showing the desired deletion. **c**, Tumour-free survival of mice with the indicated genotype (log-rank test). **d**, **e**, The extent of 11B3 deletion in non-tumorigenic pre-B cells (*Vav1-cre;11B3$^{fl/+}$*) and in lymphomas arising in *Eμ-Myc;Vav1-cre;11B3$^{fl/+}$* mice was determined by semi-quantitative PCR using mixed genomic DNA from *11B3$^{+/\Delta}$* ES cells to *11B3$^{fl/+}$* cells at different ratios (10% or 20%) (**d**), and qPCR (**e**; two-tailed *t*-test). Sample names correspond to the mouse identifier. Error bars represent standard deviation (s.d.). **f**, Copy number profile of mouse chromosome 11 as determined by low-pass whole genome sequencing of 11B3-deleted lymphoma cells obtained from **c**. Red arrows highlight the 11B3 region. **g**, Resulting *Trp53* status upon LOH from tumours arising from heterozygous chromosome 11B3 deletion (left) or those originating from heterozygous *Trp53* deletion (middle) or point mutation (right). UPD, uniparental disomy. ***$P < 0.001$.

hypoxanthine–aminopterin–thymidine (HAT) medium, and subjected to a polymerase chain reaction (PCR) analysis to discriminate between *cis* and *trans* recombination events (Extended Data Fig. 2c). This readily identified embryonic stem (ES) cell clones harbouring *loxP* sites flanking 11B3 in *cis* and revealed that 11B3 deletion is not deleterious to ES cells (data not shown). We refer to the appropriately targeted allele above as *11B3^{flox}* (*11B3^{fl}*).

11B3^{fl} mice were produced by blastocyst injection and crossed to a variety of constitutive and haematopoietic-directed Cre mouse lines. We never observed viable progeny harbouring a recombined 11B3 deletion arising from *11B3^{fl}* crosses with *Ella-cre* or constitutive *CAG-cre* mice, implying that heterozygous deletion of the 11B3 interval confers embryonic lethality. However, double-mutant progeny harbouring the *cre* transgene and an unrecombined *11B3^{fl}* allele were produced (Extended Data Table 1), perhaps surviving owing to inefficient recombination between the two distant (~4 Mb) *loxP* sites.

As in ES cells, somatic 11B3 deletion in the haematopoietic compartment was not an obligate cell lethal event; thus, recombined cells were detected in the peripheral blood of *11B3$^{fl/+}$* mice crossed to strains harbouring *Cd19-cre*, *Mx1-cre* or *Vav1-cre* alleles (Extended Data Fig. 3a). Nevertheless, the apparent recombination frequency was substantially lower than observed in progeny of conditional *Trp53*-knockout mice crossed to the same strains (20% versus 100%; Extended Data Fig. 3b, c). While such differences can complicate direct comparisons of tumour onset between *11B3^{fl}* and *Trp53^{fl}* animals, we reasoned that changes in the fraction of 11B3-deleted cells over time should indicate whether 11B3 loss provides a competitive advantage during tumorigenesis.

We first tested whether somatic deletion of 11B3 could drive cancer development in the *Eμ-Myc* transgenic model of non-Hodgkin lymphoma, as *Trp53* deletion potently accelerates lymphomagenesis in this model[16,17] and because 17p alterations are associated with adverse prognosis in the corresponding human disease[18] (Extended Data Fig. 1c). Accordingly, *Eμ-Myc* mice were crossed to the *11B3^{fl}* allele and a *Vav1-cre* transgenic strain, and the resulting progeny were monitored for tumour onset (Fig. 2c). Mice harbouring the *11B3^{fl}* allele developed lymphomas much more rapidly than controls (59 versus 130 days, $P < 0.001$), clearly indicating that loss of the 11B3 region can promote tumorigenesis.

Paradoxically, *Eμ-Myc;Trp53$^{fl/+}$;Vav1-cre* mice developed lymphomas even more rapidly than *Eμ-Myc;11B3$^{fl/+}$;Vav1-cre* animals (Extended Data Fig. 3d). While this observation is consistent with a potentially negative impact of 11B3 deletion on cellular fitness, it might also reflect the nearly fivefold reduced recombination efficiency of the *11B3^{fl}* versus *Trp53^{fl}* alleles. Consistent with the idea of reduced recombination efficiency, semi-quantitative and quantitative (q)PCR analysis indicated a massive enrichment in the fraction of 11B3-deleted cells in lymphomas compared with the premalignant setting (~100% versus 15%; Fig. 2d, e), which was confirmed by genome sequencing (Fig. 2f). Although lymphomas arising in the *Trp53$^{fl/+}$* and *11B3$^{fl/+}$* animals were both highly disseminated, 11B3-deleted lymphomas typically presented

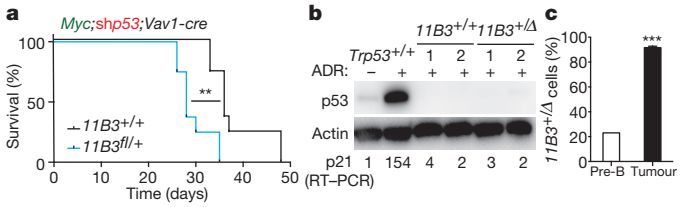

Figure 3 | 11B3 deletion can accelerate lymphomagenesis through p53-independent mechanisms. a, Kaplan–Meier lymphoma-free survival curve of recipient mice receiving *Vav1-cre;11B3*$^{fl/+}$ or *Vav1-cre;11B3*$^{+/+}$, transduced simultaneously with a mouse *Myc* cDNA and an shRNA against *Trp53* (sh*p53*). $n = 8$ per genotype. $^{**}P < 0.01$ (log-rank test). **b**, The expression levels of *Trp53* and *p21* after ADR treatment of resulting lymphoma cells as detected by immunoblotting and RT–qPCR, respectively. *p21* levels were normalized to untreated *Trp53*$^{+/+}$ lymphomas. Shown are representative results ($n = 8$ per cohort). **c**, qPCR analysis to determine the percentage of chromosome 11B3 deletion in pre-B cells (transduced cells before transplantation; $n = 3$) and resulting lymphomas ($n = 5$) from the experiment in **a**. $^{***}P < 0.001$ (two-tailed *t*-test).

as a more mature B-cell type and showed enhanced resistance to certain chemotherapeutic agents (Extended Data Fig. 4a–c). Thus, 11B3 deletion confers a selective advantage during lymphomagenesis and produces phenotypes distinct from a *Trp53*-null setting.

p53 is induced after DNA damage, when it activates transcription of target genes involved in cell cycle arrest, apoptosis, and other cellular processes[19,20]. Strikingly, all 11B3-deleted lymphomas showed either high or undetectable levels of p53 protein, and none were capable of inducing the p53 transcriptional target *p21* (also known as *Cdkn1a*) after treatment with the DNA-damaging chemotherapeutic drug adriamycin (ADR). Such a pattern is reminiscent of lymphoma cells that acquire inactivating *Trp53* mutations[21,22] and indeed, most 11B3-deleted lymphomas (75%) acquired missense or nonsense mutations in the remaining wild-type *Trp53* allele (Extended Data Fig. 4f). Other 11B3-deleted lymphomas displayed no p53 activity, suggesting that each acquired some other mutational or epigenetic event that disabled the intact wild-type *Trp53* allele. Regardless, the majority of 11B3-deleted lymphomas display chromosome configurations analogous to the common *TP53* mutation/deletion events observed in human cancers (Fig. 1a and Fig. 2g).

We also tested the mechanisms of loss of heterozygosity (LOH) arising in conventional *Trp53*-mutant mouse models. To this end, we generated *Eμ-Myc* strains with the following additional alleles: *Trp53*$^{+/-}$, *Vav1-cre;Trp53*$^{fl/+}$, *Vav1-cre;Trp53*$^{LSL\text{-}R270H/+}$, or *Vav1-cre;Trp53*$^{LSL\text{-}R172H/+}$, and analysed the fate of the remaining *Trp53* allele upon lymphoma manifestation using a qPCR assay to detect the copy number of select regions flanking *Trp53*. In these models LOH clearly does not involve deletion of the remaining *Trp53* locus, as the genes proximal and distal to *Trp53* (for example, *Eif5a* and *Sco1/Alox12*, respectively) remained diploid in all cases (Extended Data Fig. 5a). Instead, this analysis suggests that LOH occurs through duplication of the targeted mutant *Trp53* allele, a conclusion that was confirmed by analysis of polymorphic markers in this region (Fig. 2g and Extended Data Fig. 5b, c). While such 17p configurations occur in human tumours, they are less frequent than those involving large deletions (see Fig. 1a).

Role of 11B3 deletion in lymphomagenesis

Although the data described earlier demonstrate that 11B3 deletion can contribute to tumorigenesis, the differences in recombination frequencies between the conditional 11B3 and *Trp53* alleles made it impossible to assess whether other genes in the 11B3 deletion contribute to its effects. To mitigate this caveat without extensive strain intercrossing, we exploited the capability of shRNAs to suppress gene expression in *trans*, hypothesizing that any phenotypic differences arising between wild-type and 11B3-deleted cells expressing a potent *Trp53* shRNA would be independent of *Trp53*. As immunoblotting and qPCR with reverse transcription (RT–qPCR) analysis confirmed that our *Trp53* shRNA was equally capable of disabling *Trp53* in pre-B cells harbouring one or two *Trp53* alleles (Extended Data Fig. 6), we co-transduced pre-B cells derived from the bone marrow of *Vav1-cre* and *Vav1-cre;11B3*$^{fl/+}$ mice with a *Myc* complementary DNA (linked to GFP) and the *Trp53* shRNA (linked to *mCherry*) and studied tumorigenesis upon their transplantation into irradiated recipient mice.

Mice receiving cells harbouring the conditional 11B3 deletion and the *Trp53* shRNA developed tumours more rapidly than those transplanted with cells harbouring the *Trp53* shRNA alone (Fig. 3a; median onset 28 versus 36 days, $P < 0.01$). In both the *11B3*$^{fl/+}$ and *11B3*$^{+/+}$ settings, the disease presented as an aggressive B-cell malignancy (data not shown) in which p53 protein and activity were undetectable (Fig. 3b). Furthermore, the subsequent lymphomas were double positive for GFP and mCherry, indicating that they retained the *Myc* cDNA and *Trp53* shRNA (data not shown). While only 15–20% of the premalignant cells underwent 11B3 recombination, almost all of the resulting lymphoma cells harboured this deletion (Fig. 3c). Thus, 11B3 deletion confers a strong selective advantage even in the absence of detectable p53 function.

To identify genetic elements within the 11B3 interval that act together with *Trp53* to suppress lymphoma development, we first took a candidate gene approach. We noted that virtually all lymphoma-associated 17p deletions encompass both *TP53* and *E1F5A* (see Fig. 1b), the latter gene also having been identified as a tumour suppressor that promotes apoptosis[11]. To examine interactions between these genes during lymphomagenesis, validated shRNAs targeting *Trp53* and/or *Eif5a*, co-expressed in tandem, were introduced into *Eμ-Myc* haematopoietic stem and progenitor cells (HSPCs) and then transplanted into syngeneic recipients. As expected, suppression of either *Trp53* or *Eif5a* accelerated lymphomagenesis relative to controls, which did not develop tumours over the time of evaluation (Fig. 4a; median onset 56 and 99.5 days, respectively). Still, co-suppression of both *Trp53* and *Eif5a* produced lymphomas even more rapidly (median onset 45 days). Apparently, premalignant cells co-suppressing *Trp53* and *Eif5a* shRNAs have an increased selective advantage compared with cells expressing either shRNA alone, a suggestion that was confirmed by an *in vivo* competition assay (Extended Data Fig. 7) and apoptosis measurements in premalignant cells (Fig. 4b)[16,23,24]. Although our shRNA technology cannot precisely mimic the gene dosage produced by a heterozygous gene deletion, these data identify *Eif5a* as a second gene in the 11B3 interval that can contribute to its activity.

To test whether additional 17p13 genes have a role, we generated a shRNA library targeting the ~100 protein-coding genes in the 11B3 region (exclusive of *Trp53* and *Eif5a*) and screened it for tumour-promoting activity in HSPC transplantation assays (Fig. 4c; 17p13 shRNA library detailed in Supplementary Table 1). Compared with controls, these libraries accelerated lymphomagenesis in recipient mice, implying that one or more shRNAs conferred a selective advantage (Fig. 4d). To identify such shRNAs, PCR products amplified from genomic DNA were subject to deep sequencing and the abundance of each shRNA compared to the initial pool. Forty shRNAs targeting 17 genes were enriched in tumours compared to the injected population (Supplementary Table 1).

Among the potential candidates, two shRNAs targeting *Alox15b* (sh*Alox15b.1252* and sh*Alox15b.2865*), showed a 245- and 50-fold enrichment, respectively, compared with their representation in the initial library (Extended Data Fig. 8a). We thus tested whether suppression of *Alox15b* alone or in combination with *Trp53* could accelerate tumorigenesis as was done for *Eif5a*. Recipients of HSPCs targeted with *Alox15b* shRNAs had significantly shorter lymphoma-free survival than sh*Ren* controls (Fig. 4e), and those receiving HSPCs harbouring *Alox15b-Trp53* tandem shRNA showed a further acceleration over sh*Trp53*-sh*Ren* controls (Fig. 4f).

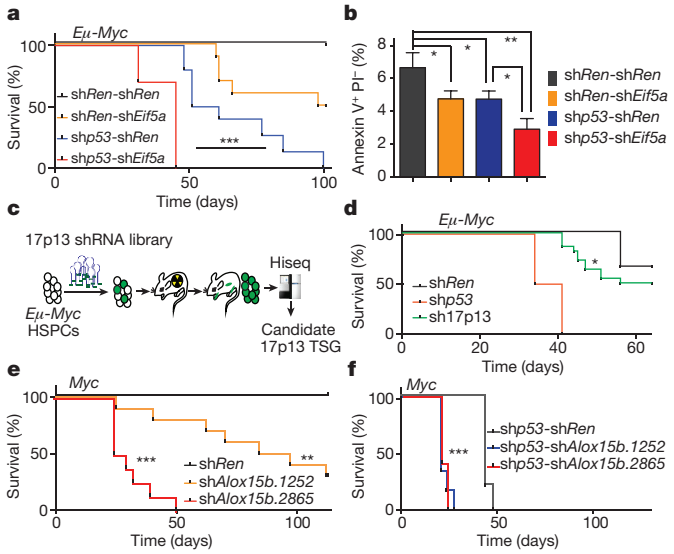

Figure 4 | 11B3 encodes multiple genes whose attenuation cooperates with *Trp53* loss to drive lymphoma. a, Kaplan–Meier lymphoma-free survival of recipient mice transplanted with *Eμ-Myc* HSPCs with various GFP-linked tandem shRNAs. sh*p53* indicates sh*Trp53*. $n = 10$ per group. **b**, Annexin V staining of *Eμ-Myc* pre-B cells transduced with the indicated tandem shRNAs constructs. $n = 3$. Result represents at least two independent experiments. PI, propidium iodide. **c**, **d**, *In vivo* shRNA screen to identify potential tumour suppressors on chromosome 17p13 (**c**) and resulting tumour-free survival curve of mice receiving HPSCs transduced with shRNA pools (**d**). Hiseq, high-throughput sequencing; TSG, tumour suppressor gene. **e**, **f**, Kaplan–Meier tumour-free survival curve of recipient mice transplanted with pre-B cells co-infected with *Myc* and the indicated shRNAs (**e**; $n = 10$), or infected with Myc-linked tandem shRNAs (**f**; $n = 6$). **a**, **d**–**f**, Log-rank test. **b**, Unpaired two-tailed *t*-test, error bars represent s.d. $^*P < 0.05$; $^{**}P < 0.01$; $^{***}P < 0.001$.

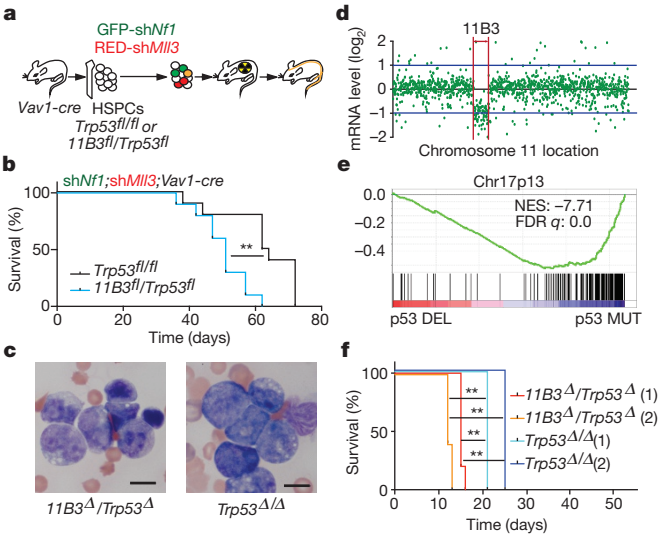

Figure 5 | Chromosome 11B3 deletion acts beyond *Trp53* loss to drive myeloid leukaemia. a, AML generation by HSPC isolation (*Vav1-cre;Trp53*$^{fl/fl}$ or *Vav1-cre;11B3*^{fl}*/Trp53*^{fl}), co-transduction with a GFP-linked *Nf1* shRNA and an mCherry-linked *Mll3* shRNA, and transplantation into sublethally irradiated recipients ($n = 10$ per group). **b**, Post-transplant, leukaemia-free survival $^{**}P < 0.01$ (log-rank test). **c**, Blood smear of moribund mice (**b**) that is representative of all animals analysed in each genotype ($n = 4$). **d**, RNA-seq comparison of chromosome 11 gene-expression levels between the *11B3*$^{\Delta}$*/Trp53*$^{\Delta}$ and *Trp53*$^{\Delta/\Delta}$ leukaemia generated in **b** ($n = 4$). **e**, Gene set enrichment analysis of genes on chromosome 17p13 in chromosome 17p-deleted human AML compared to those with *TP53* mutations but without 17p deletions. FDR, false discovery rate; NES, normalized enrichment score. **f**, Kaplan–Meier survival curve of secondary transplants from two independent primary leukaemias of each genotype in **a**, **b**. $n = 5$ in each cohort. $^{**}P < 0.01$ (log-rank test).

Partial knockdown of *Alox15b* by shRNAs in NIH3T3 cells resulted in accumulation of its substrate, arachidonic acid (AA) (Extended Data Fig. 8b, c), and higher AA levels were detected in 11B3-deleted lymphoma cells compared with their *Trp53*-null counterparts (Extended Data Fig. 8d). Interestingly, AA suppresses apoptosis in certain cancer cells[25] and, in agreement, exogenous AA inhibited apoptosis of pre-B cells in a dose-dependent manner (Extended Data Fig. 8e). While a complete mechanistic understanding of its effects will require further work, these studies pinpoint *Alox15b* as an additional tumour suppressor in the 11B3 region. Intriguingly, shRNAs targeting two other Alox family genes adjacent to *Alox15b* were enriched in our screen (*Alox12b*, *Alox3e*), raising the possibility that 17p deletion coordinately attenuates the output of this gene family. Additionally, beyond protein-coding genes, the reduced dosage of non-coding RNAs not tested in our screen might contribute to the activity of 17p deletions[26].

11B3 deletion contributes to AML

We also asked whether 11B3 loss would enhance tumorigenesis in a genetically and pathologically accurate mouse model of complex-karyotype AML, an invariably lethal leukaemia subtype[9,27,28]. In this disease, *TP53* lesions often co-occur with *NF1* loss and deletions on 5q and/or 7q, which can be approximated in mice transplanted with *Trp53*$^{-/-}$ HSPCs co-expressing shRNAs targeting *Nf1* and *Mll3* (also known as *Kmt2c*) (encoded on human 7q36)[29]. Taking advantage of the flexibility of this model, we compared disease onset and pathology in mice transplanted with sh*Nf1*-sh*Mll3*-transduced HSPCs derived from either *Vav1-cre;Trp53*$^{fl/fl}$ or *Vav1-cre;11B3*^{fl}*/Trp53*^{fl} mice (Fig. 5a).

These experiments revealed a clear and substantial p53-independent effect of 11B3 deletion on leukaemia development. Indeed, despite the reduced recombination frequency of the 11B3 allele (Extended Data Fig. 9a), recipients of *Vav1-cre;11B3*^{fl}*/Trp53*^{fl} HSPCs had a significantly decreased survival compared with recipients of *Vav1-cre;Trp53*$^{fl/fl}$ HSPCs, and succumbed to an aggressive form of AML (Fig. 5b, c and Extended Data Fig. 9b–d; median overall survival 62 versus 81 days, $P = 0.002$). RNA-sequencing (RNA-seq) analysis confirmed that 11B3 genes were underexpressed in 11B3-deleted AML cells compared with those in the *Trp53*-null setting (Fig. 5d), and gene set enrichment analysis revealed that transcriptional profiles of human 17p13 genes are downregulated in human AMLs harbouring 17p13 deletions (Fig. 5e). Moreover, 11B3-deleted AMLs were capable of serial transplantation into secondary recipients, where they promoted disease more rapidly than their *Trp53*-null counterparts (Fig. 5f). Finally, while the *Trp53*$^{-/-}$ AMLs are sensitive to the BET-protein inhibitor JQ1 (ref. 29), the corresponding *11B3*$^{-}$*/Trp53*$^{-}$ AML showed reduced sensitivity (Extended Data Fig. 9e, f). Hence, 11B3 deletions contribute p53-independent phenotypes to AML.

Discussion

This study provides compelling evidence that 17p deletion confers phenotypes beyond those achieved through *TP53* loss alone. When considered in light of the established gain-of-function properties of certain missense *Trp53* mutations, our results imply that the most frequent somatic event in cancer contributes multiple activities that act independently of *Trp53* inactivation to drive tumorigenesis. It therefore seems likely that tumours harbouring *TP53* lesions—typically considered a uniform entity—produce distinct phenotypes owing to the nature of the *TP53* mutation and the extent of 17p deletion. As such, the models described here will be useful for dissecting precisely how different 17p configurations affect disease onset and ultimately impact therapy response. More broadly, our study

provides direct *in vivo* evidence that segmental deletion events can arise owing to the selective advantage of disrupting multiple genes and provides a blueprint to dissect these common but understudied cancer-promoting lesions.

Online Content Methods, along with any additional Extended Data display items and Source Data, are available in the online version of the paper; references unique to these sections appear only in the online paper.

Received 29 April 2015; accepted 20 January 2016.
Published online 16 March 2016.

1. Hanahan, D. & Weinberg, R. A. Hallmarks of cancer: the next generation. *Cell* **144,** 646–674 (2011).
2. Zender, L. *et al.* An oncogenomics-based *in vivo* RNAi screen identifies tumor suppressors in liver cancer. *Cell* **135,** 852–864 (2008).
3. Xue, W. *et al.* A cluster of cooperating tumor-suppressor gene candidates in chromosomal deletions. *Proc. Natl Acad. Sci. USA* **109,** 8212–8217 (2012).
4. Solimini, N. L. *et al.* Recurrent hemizygous deletions in cancers may optimize proliferative potential. *Science* **337,** 104–109 (2012).
5. Davoli, T. *et al.* Cumulative haploinsufficiency and triplosensitivity drive aneuploidy patterns and shape the cancer genome. *Cell* **155,** 948–962 (2013).
6. Miller, L. D. *et al.* An expression signature for p53 status in human breast cancer predicts mutation status, transcriptional effects, and patient survival. *Proc. Natl Acad. Sci. USA* **102,** 13550–13555 (2005).
7. Petitjean, A., Achatz, M. I., Borresen-Dale, A. L., Hainaut, P. & Olivier, M. *TP53* mutations in human cancers: functional selection and impact on cancer prognosis and outcomes. *Oncogene* **26,** 2157–2165 (2007).
8. Gao, J. *et al.* Integrative analysis of complex cancer genomics and clinical profiles using the cBioPortal. *Sci. Signal.* **6,** pl1 (2013).
9. Wattel, E. *et al.* p53 mutations are associated with resistance to chemotherapy and short survival in hematologic malignancies. *Blood* **84,** 3148–3157 (1994).
10. El-Ghammaz, A. M., Abdelwahed, E., Mostafa, N. N. & Mansour, D. A. *De novo* deletion 17p13.1 as a predictor for disease progression in chronic lymphocytic leukemia. *Clin. Exp. Med.* **15,** 493–499 (2015).
11. Scuoppo, C. *et al.* A tumour suppressor network relying on the polyamine–hypusine axis. *Nature* **487,** 244–248 (2012).
12. Wales, M. M. *et al.* p53 activates expression of *HIC-1*, a new candidate tumour suppressor gene on 17p13.3. *Nature Med.* **1,** 570–577 (1995).
13. Ahn, Y. H. *et al.* Map2k4 functions as a tumor suppressor in lung adenocarcinoma and inhibits tumor cell invasion by decreasing peroxisome proliferator-activated receptor γ2 expression. *Mol. Cell. Biol.* **31,** 4270–4285 (2011).
14. Mermel, C. H. *et al.* GISTIC2.0 facilitates sensitive and confident localization of the targets of focal somatic copy-number alteration in human cancers. *Genome Biol.* **12,** R41 (2011).
15. Adams, D. J. *et al.* Mutagenic insertion and chromosome engineering resource (MICER). *Nature Genet.* **36,** 867–871 (2004).
16. Schmitt, C. A. *et al.* Dissecting p53 tumor suppressor functions *in vivo*. *Cancer Cell* **1,** 289–298 (2002).
17. Eischen, C. M., Weber, J. D., Roussel, M. F., Sherr, C. J. & Cleveland, J. L. Disruption of the ARF–Mdm2–p53 tumor suppressor pathway in Myc-induced lymphomagenesis. *Genes Dev.* **13,** 2658–2669 (1999).
18. Monti, S. *et al.* Integrative analysis reveals an outcome-associated and targetable pattern of p53 and cell cycle deregulation in diffuse large B cell lymphoma. *Cancer Cell* **22,** 359–372 (2012).
19. Levine, A. J. & Oren, M. The first 30 years of p53: growing ever more complex. *Nature Rev. Cancer* **9,** 749–758 (2009).
20. Vousden, K. H. & Prives, C. Blinded by the light: the growing complexity of p53. *Cell* **137,** 413–431 (2009).
21. Olive, K. P. *et al.* Mutant p53 gain of function in two mouse models of Li–Fraumeni syndrome. *Cell* **119,** 847–860 (2004).
22. Hanel, W. *et al.* Two hot spot mutant p53 mouse models display differential gain of function in tumorigenesis. *Cell Death Differ.* **20,** 898–909 (2013).
23. Hemann, M. T. *et al.* Suppression of tumorigenesis by the p53 target PUMA. *Proc. Natl Acad. Sci. USA* **101,** 9333–9338 (2004).
24. Kelly, G. L. *et al.* Targeting of MCL-1 kills MYC-driven mouse and human lymphomas even when they bear mutations in *p53*. *Genes Dev.* **28,** 58–70 (2014).
25. Tang, D. G. *et al.* Suppression of W256 carcinosarcoma cell apoptosis by arachidonic acid and other polyunsaturated fatty acids. *Int. J. Cancer* **72,** 1078–1087 (1997).
26. Balatti, V. *et al. TCL1* targeting *miR-3676* is codeleted with tumor protein p53 in chronic lymphocytic leukemia. *Proc. Natl Acad. Sci. USA* **112,** 2169–2174 (2015).
27. Slovak, M. L. *et al.* Karyotypic analysis predicts outcome of preremission and postremission therapy in adult acute myeloid leukemia: a Southwest Oncology Group/Eastern Cooperative Oncology Group Study. *Blood* **96,** 4075–4083 (2000).
28. Byrd, J. C. *et al.* Pretreatment cytogenetic abnormalities are predictive of induction success, cumulative incidence of relapse, and overall survival in adult patients with de novo acute myeloid leukemia: results from Cancer and Leukemia Group B (CALGB 8461). *Blood* **100,** 4325–4336 (2002).
29. Chen, C. *et al.* MLL3 is a haploinsufficient 7q tumor suppressor in acute myeloid leukemia. *Cancer Cell* **25,** 652–665 (2014).

Supplementary Information is available in the online version of the paper.

Acknowledgements We thank J. P. Morris, L. Dow, D. Tschaharganeh, E. Manchado, T. Kitzing, E. Loizou and other Lowe laboratory members for their critical discussions and technical help, C. J. Sherr for invaluable advice, L. Dai and M. Tang for liquid chromatography–mass spectrometry support, and Y. Park and S. Kim for their help in constructing the 11B3 mouse model. This work was supported by a programme project and an R01 grant from the National Cancer Institute (S.W.L.), a Center grant for Cancer Target Discovery and Development (S.W.L.), and a Memorial Sloan Kettering Cancer Center Support Grant. Y.L. was supported by an American Association for Cancer Research Millennium Fellowship in Lymphoma Research. C.C. is supported by the Thousand Young Talents Plan and the National Natural Science Foundation of China (81522003, 81570150). S.W.L. is the Geoffrey Beene Chair for Cancer Biology and a Howard Hughes Medical Institute Investigator.

Author Contributions Y.L. and S.W.L. designed the experiments. Y.L., C.C., S.A., Z.X. and L.C. performed the experiments. Y.L., C.C., Z.X., T.N. and S.W.L. analysed data. Y.L., C.S. and A.A.M. designed the 11B3 model, Y.L., C.S., J.G., B.B., E.R.K., T.B., B.S., T.N., Q.W., N.S. and R.L.L. contributed to the human cancer genomic analysis. Y.L., C.C., C.D.R. and S.W.L. organized data and wrote the manuscript.

Author Information 17p13 shRNA library specification is provided in Supplementary Information. The raw and analysed RNA sequence data have been deposited in the Gene Expression Omnibus under accession number GSE69654. Reprints and permissions information is available at www.nature.com/reprints. The authors declare no competing financial interests. Readers are welcome to comment on the online version of the paper. Correspondence and requests for materials should be addressed to S.W.L. (lowes@mskcc.org).

METHODS

Genomic analyses of human cancers. The data on *TP53* mutations (including allele frequency) and CNVs in pan-tumours and AML are derived from The Cancer Genome Atlas (TCGA) data in the cBioPortal for Cancer Genomics (http://www.cbioportal.org/; accessed on 29 October 2014). Only sequenced samples with allele frequency information provided were included in our analysis. Considering potential normal tissue contamination, samples with *TP53* mutation allele frequency above 0.6 were considered as a homozygous mutation. The SNP data were visualized in IGV and statistics for AML outcome were analysed in Prism 6. Since cBioPortal only has a few non-Hodgkin lymphoma cases available, we used published data to extract *TP53* mutation and deletion information[18,30–34]. Clinical outcomes were annotated from follow-up data available within the Gene Expression Omnibus GSE34171 series.

CNV analysis was performed using published AML and DLBCL tumour copy number data in Affymetrix SNP Array 6.0 .cel format (http://cancergenome.nih.gov/)[18,35–37] according to GISTIC2.0 (ref. 14). Specifically, the following GISTIC parameters and values were used following the latest TCGA Copy Number Portal analysis version (3 November 2014 stddata__2014_10_17; http://www.broadinstitute.org/tcga/gistic/browseGisticByTissue): core GISTIC version 2.0.22; reference genome build hg19; amplification threshold 0.1; deletion threshold 0.1; high-level amplification threshold 1.0; high-level deletion threshold 1.0; broad length cut-off 0.50; peak confidence level 0.95; cap 1.5; gene-GISTIC, true; arm-level peel-off, true; significance threshold 0.25; join segment size 8; X chromosome removed, false; maximum segments per sample 2,000; minimum samples per disease 40.

Conditional 11B3-knockout model. To create a conditional 11B3 chromosome deletion, the MICER strategy was used[15]. Briefly, MICER clones MHPN91j22 (centromeric to *Sco1*) and MHPP248j19 (telomeric to *Alox12*) (Sanger Institute) were introduced into AB2.2 ES cells (129S5 strain, Sanger Institute) by sequential electroporation, followed by G418 (neomycin; 180 μg ml^{-1}) and puromycin (1 μg ml^{-1}) selection, respectively. Successful recombination events were confirmed by Southern blotting using the hybridized probes designated in Supplementary Table 2 as described[38]. The *cis*- and *trans*-localizations of two *loxP* sites in doubly targeted ES cells were further distinguished by PCR with df-F and df-R, or dp-F and dp-R (Supplementary Table 2), respectively, after Adeno-*cre* infection and HAT (Gibco) selection. Correct *cis*-ES clones in which two *loxP* sites were integrated into the same allele were used to generate chimaera mice by blastocyst injection. The F1 pups were genotyped with 11B3-F and 11B3-R primers (Supplementary Table 2) and those positive backcrossed to C57BL/6 mouse strains for more than 10 generations.

Mice. All of the mouse experiments were approved by the Institutional Animal Care and Use Committee at the Memorial Sloan Kettering Cancer Center. *Eμ-Myc*, *Vav1-cre*, *Ella-cre*, *Trp53*$^{LSL\text{-}R270H/+}$, *Trp53*$^{LSL\text{-}R72H/+}$, *Trp53*$^{+/-}$, *Trp53*$^{fl/+}$ and *Rag1*$^{-/-}$ mice were ordered from Jackson Laboratories[21,39–44] and the *Arf*$^{+/-}$ mouse strain is a gift from C. Sherr[45]. *Eμ-Myc* mice with different *Trp53* alterations were monitored weekly with disease state being defined by palpable enlarged solid lymph nodes and/or paralysis. Tumour monitoring was done as blinded experiments. For lymphoma generated by transplantation, 1 million *Eμ-Myc* HPSCs from embryonic day (E)13.5 fetal liver or autoMACS-purified B220$^+$ B progenitor cells isolated from 6–8-week mouse bone marrow were transduced with retroviruses, followed by tail-vein injection into sublethally irradiated (6 Gy, Cs137) C57BL/6 mice (Taconic; 6–8-week old, female, 5–10 mice per cohort)[11,46]. All recipient mice were randomly divided into subgroups before transplantation and monitored as described earlier. The generation of AML proceeded as previously reported[29]. Briefly, retrovirally infected c-Kit$^+$ haematopoietic stem and progenitor cells were transplanted into sublethally irradiated (6 Gy, Cs137) C57BL/6 mice, followed by routine monitoring of peripheral blood cell counts and Giemsa–Wright blood smear staining. For secondary transplantation experiments, 1 million leukaemia cells were transplanted into sublethally irradiated (4.5 Gy) mice. The immunophenotypes of resulting lymphomas and leukaemias were determined by flow cytometry as previously reported using antibodies purchased from eBioscience[11,29]. Statistical analysis of all survival data was carried out using the log-rank test from Prism 6. No statistical methods were used to predetermine sample size.

Retroviral constructs. MSCV-Myc-IRES-GFP and MLS-based retroviral constructs harbouring a GFP or mCherry fluorescent reporter and targeting *Ren*, *Trp53*, *Eif5a*, *Nf1* or *Mll3* have all been reported before[11,29,47]. For the tandem shRNA experiments performed in Fig. 3, mirE-based shRNAs targeting two different genes were cloned into an MLS-based vector in an analogous fashion to what has been previously described[48,49]. Retrovirus packaging and infection of HSPCs was done as previously reported[11,29].

Apoptosis assay. B220$^+$ cells were isolated from the bone marrow of 6-week-old *Eμ-Myc* mice by autoMACS positive selection with anti-B220 microbeads (Miltenyi Biotech). After overnight culture, cells were infected with retroviruses carrying the indicated shRNAs. Two days after infection, 0.5×10^6 cells were washed with PBS followed by annexin V buffer (10 mM HEPES, 140 mM NaCl, 25 mM $CaCl_2$, pH 7.4), and incubated at room temperature with Pacific Blue annexin V (BD Biosciences) and propridium iodide (PI; 1 μg ml^{-1}; Sigma-Aldrich) for 15 min and analysed on a LSR II flow cytometer (BD Biosciences). For arachidonic acid treatment, pre-B cells were cultured out from bone marrow cells in pre-B cell medium (RPMI1640, 10% FBS, 1% penicillin/streptomycin, 50 μM β-mercaptoethanol, 3 ng ml^{-1} IL-7). After 3 days culture, pre-B cells were treated with a series concentration of arachidonic acid (Cayman Chemical) for 20 h, followed by annexin V staining as described earlier.

Immunoblotting. Lymphoma cells isolated from lymph nodes of diseased animals were treated with vehicle (PBS) or 1 μg ml^{-1} adriamycin for 4 h. Whole cell lysates were extracted in cell lysis buffer (Cell Signaling Technology) supplemented with protease inhibitors (Roche), followed by SDS–PAGE gel electrophoresis and blotting onto PVDF membranes (Millipore). *Eμ-Myc;Arf*$^{-/-}$ lymphoma cell lines were used as a positive control for p53 induction. The p53 antibody used was obtained from Novocastra (NCL-p53-505) and horseradish peroxidase (HRP)-conjugated β-actin antibody from Sigma (AC-15). Alox15b expressions were examined in NIH3T3 cells, which were infected by shRNAs targeting *Ren* or *Alox15b* and then selected by G418. Anti-Alox15b antibody is from Sigma (SAB2100110), and HRP-conjugated GAPDH antibody is from ThermoFisher Scientific (MA5-15738-HRP).

Gene expressing profiling. RNA-seq and data analysis were performed by the Integrated Genomic and Bioinformatics core at the Memorial Sloan Kettering Cancer Center. Briefly, total RNA from *11B3*^{fl}/*Trp53*^{fl};sh*Nf1*;sh*Mll3*;*Vav1-cre* or *Trp53*$^{fl/fl}$;sh*Nf1*;sh*Mll3*;*Vav1-cre* leukaemia cells (four lines per cohort), isolated from the bone marrow of moribund mice, was isolated by Trizol extraction (Life Technologies). After ribogreen quantification (Life Technologies) and quality control on an Agilent BioAnalyzer, 500 ng of total RNA (RNA integrity number > 8) underwent polyA selection and Truseq library preparation according to instructions provided by Illumina (TruSeq RNA Sample Prep Kit v.2) with 6 cycles of PCR. Samples were barcoded and run on a Hiseq 2500 in a 50 bp/50 bp paired-end run, using the TruSeq SBS Kit v.3 (Illumina). An average of 45 million paired reads were generated per sample. At the most the ribosomal reads represented 0.1% and the percentage of mRNA bases was close to 65% on average. The output from the sequencers (FASTQ files) was mapped to the mouse genome (mm9) using the rnaStar (https://code.google.com/p/rna-star/) aligner, with the two-pass mapping methods. After mapping, the expression counts of each individual gene were computed using HTSeq (http://www-huber.embl.de/users/anders/HTSeq), followed by normalization and differential expression analysis among samples using the R/Bioconductor package DESeq (http://www-huber.embl.de/users/anders/DESeq). Gene set enrichment analysis (GSEA) was performed with Broad's GSEA algorithm.

Quantitative PCR. A list of all primers used for PCR analysis is given in Supplementary Table 2. For detection and quantification of 11B3 recombination/deletion two methods were employed. In both cases genomic DNA (gDNA) was extracted from lymphoma or leukaemia cells using Puregene DNA purification kit (Qiagen). Initially, semi-quantitative PCR was used to detect the recombined 11B3 allele using primers df-F and df-R, generating a 2.2 kb product (Fig. 2d). The estimated frequency of recombination was determined by dropping gDNA from *11B3*$^{+/-}$ into *11B3*$^{fl/+}$ at various ratios. For qPCR of the 11B3 deletion (Fig. 2e), SYBR Green PCR Master Mix (Applied Biosystems) was used and cycling and analysis was carried out on a ViiA 7 (Applied Biosystems). Primers 11B3-Q-F and 11B3-Q-R were used to detect the floxed allele, and to estimate the frequency of 11B3 deletion. Allelic frequency in UPD analysis (Extended Data Fig. 5a) was determined similarly, in this case with serial dilution of wild-type gDNA into DNase-free water to construct a standard curve. Two-tailed *t*-test is used for statistics analysis by Prism 6. For *p21* gene expression examination by RT–qPCR, RNA was isolated with Trizol, cDNA was synthesized with SuperScript III First-Strand Synthesis System (Life Technologies) and qPCR was performed as described earlier with primers p21-Q-F and p21-Q-R.

***Trp53* genomic DNA sequencing.** *Trp53* exons (2–10) were amplified from genomic DNAs of 11B3-deleted lymphomas by PCR (see Supplementary Table 2 for primer sequences) and subjected to Sanger sequencing. Mutations were called only if detected in sequencing reads carried out in the forward and reverse direction.

SNP analysis. SNP analysis of isolated lymphoma (tumour) or tail (normal) genomic DNAs from the same tumour-bearing mouse were carried out by Charles River laboratory. Briefly, a SNP Taqman assay with competing FAM- or VIC-labelled probes was used to detect the relevant C57BL/6 and 129S SNPs (D11Mit4 and D11NDS16) as described previously[50].

Copy number profiling. Genomic DNA was extracted from freshly isolated lymphoma cells from one *Eμ-Myc;11B3*$^{fl/+}$;*Vav-cre* mice. One microgram of DNA was sonicated (17 W, 75 s) on an E220 sonicator (Covaris). Samples were subsequently

prepared using standard Illumina library preparation (end repair, poly A addition, and adaptor ligation). Libraries were purified using AMPure XP magnetic beads (Beckman Coulter), PCR enriched, and sequenced on an Illumina HiSeq instrument in a multiplexed format. Sequencing reads per sample were mapped using Bowtie with PCR duplicates removed. Approximately 2.5 million uniquely mappable reads were further processed for copy number determination using the 'varbin' algorithm[51,52] with 5,000 bins, allowing for a median resolution of ~600 kb. GC content normalization, segmentation and copy number estimation was calculated as described[53].

shRNA library construction and tumour sequencing. A custom shRNA library was designed to target mouse homologues (six shRNAs for one gene) to all human protein-coding genes on chromosome 17p13.1 from *ALOX12* to *SCO1*, except *TP53* and *EIF5A*. shRNAs were cloned into a retrovirus-based vector MLS by pool-specific PCR as previously described[11]. *Eμ-Myc* HSPCs infected with pooled shRNAs were transplanted into sublethally irradiated recipient mice. Resulting tumours were harvested, and used to extract contained shRNAs, followed by HiSeq in HiSeq 2500 (Illumina). Twenty-two oligonucleotides of shRNAs used in this study are listed in Supplementary Table 3.

LC-MS. Total lipids were extracted using Folch's method[54] and analysed by LC-MS as previously described[55]. Briefly, freshly harvested cells were homogenized by chloroform/methanol (2:1, v-v). After being washed by water, the lipid-containing chloroform phase is evaporated. Dried lipids were dissolved in 100 μl 95% acetonitrile (in H_2O), sonicated for 3–5 min, and spiked with 10 μl of 500 ng ml^{-1} deuterated internal standard solution (IS; arachidonic acid-d8; Cayman Chemical, 390010). Then, 5 μl samples were injected into Acquity ultra performance liquid chromatography (UPLC) system (Waters), equipped with Acquity UPLC BEH C18 column (100 mm × 2.1 mm I.D., 1.7 μm; Waters). Samples were washed through the column with a gradient 0.1% formic acid: acetonitrile mobile elution from 35:65 (v:v) to 5:95 for 10 min. Flow rate was 0.25 ml min^{-1}. Right after HPLC, samples were analysed in a Quattro Premier EX triple quadrupole mass spectrometer (Waters), which has electrospray negative mode and MasslynxV4.1 software. For each run, a standard curve was generated with different concentration of arachidonic acid lipid maps MS standard (Cayman Chemical, 10007268) mixed with IS (50 ng ml^{-1} final concentration). Arachidonic acid standard m/z is 303.2, and IS is 311.3.

***In vitro* drug response assays.** Three *Eμ-Myc* lymphoma cell lines generated from *Trp53$^{fl/+}$;Vav1-cre* or *11B3$^{fl/+}$;Vav1-cre* tumour-bearing mice were cultured in BCM medium (45% DMEM, 45% IMDM, 10% FBS, 2 mM glutamine, 50 μM β- mercaptoethanol, 1 × penicillin/streptomycin) in 96-well plates. Cells were treated with the indicated concentrations of 4-hydroxycyclophosphamide (Toronto Research Chemicals) or vincristine (Bedford Laboratories) for 3 days. The number of living cells was determined by PI staining and cell counting on a Guava EasyCyte (EMD Millipore). Leukaemia cell lines from *Trp53$^{\Delta/\Delta}$* or *11B3$^{\Delta}$/Trp53$^{\Delta}$*;sh*Nf1*;sh*Mll3* mice were treated with cytarabine (araC; Bedford Laboratories) or JQ1 (a gift from J. Bradner) in stem cell medium (BCM medium supplemented with 1 ng ml^{-1} IL-3, 4 ng ml^{-1} IL-6 and 10 ng ml^{-1} SCF) and cell viability after 3 days was determined similarly. All cytokines are from Invitrogen.

30. Salaverria, I. *et al.* Specific secondary genetic alterations in mantle cell lymphoma provide prognostic information independent of the gene expression-based proliferation signature. *J. Clin. Oncol.* **25,** 1216–1222 (2007).
31. Rubio-Moscardo, F. *et al.* Mantle-cell lymphoma genotypes identified with CGH to BAC microarrays define a leukemic subgroup of disease and predict patient outcome. *Blood* **105,** 4445–4454 (2005).
32. Chen, W. *et al.* Array comparative genomic hybridization reveals genomic copy number changes associated with outcome in diffuse large B-cell lymphomas. *Blood* **107,** 2477–2485 (2006).
33. Bea, S. *et al.* Diffuse large B-cell lymphoma subgroups have distinct genetic profiles that influence tumor biology and improve gene-expression-based survival prediction. *Blood* **106,** 3183–3190 (2005).
34. Mestre-Escorihuela, C. *et al.* Homozygous deletions localize novel tumor suppressor genes in B-cell lymphomas. *Blood* **109,** 271–280 (2007).
35. Rücker, F. G. *et al. TP53* alterations in acute myeloid leukemia with complex karyotype correlate with specific copy number alterations, monosomal karyotype, and dismal outcome. *Blood* **119,** 2114–2121 (2012).
36. Chigrinova, E. *et al.* Two main genetic pathways lead to the transformation of chronic lymphocytic leukemia to Richter syndrome. *Blood* **122,** 2673–2682 (2013).
37. The Cancer Genome Atlas Research Network. Genomic and epigenomic landscapes of adult de novo acute myeloid leukemia. *N. Engl. J. Med.* **368,** 2059–2074 (2013).
38. Brown, T. Southern blotting. Curr. Protoc. *Prot. Sci. 13,* 4G:A.4G.1–4G:A.4G.8 (2001).
39. Adams, J. M. *et al.* The c-*myc* oncogene driven by immunoglobulin enhancers induces lymphoid malignancy in transgenic mice. *Nature* **318,** 533–538 (1985).
40. de Boer, J. *et al.* Transgenic mice with hematopoietic and lymphoid specific expression of Cre. *Eur. J. Immunol.* **33,** 314–325 (2003).
41. Lakso, M. *et al.* Efficient *in vivo* manipulation of mouse genomic sequences at the zygote stage. *Proc. Natl Acad. Sci. USA* **93,** 5860–5865 (1996).
42. Jacks, T. *et al.* Tumor spectrum analysis in *p53*-mutant mice. *Curr. Biol.* **4,** 1–7 (1994).
43. Marino, S. & Vooijs, M., van Der Gulden, H., Jonkers, J. & Berns, A. Induction of medulloblastomas in *p53*-null mutant mice by somatic inactivation of *Rb* in the external granular layer cells of the cerebellum. *Genes Dev.* **14,** 994–1004 (2000).
44. Mombaerts, P. *et al.* RAG-1-deficient mice have no mature B and T lymphocytes. *Cell* **68,** 869–877 (1992).
45. Kamijo, T. *et al.* Tumor suppression at the mouse *INK4a* locus mediated by the alternative reading frame product p19^{ARF}. *Cell* **91,** 649–659 (1997).
46. Chien, Y. *et al.* Control of the senescence-associated secretory phenotype by NF-κB promotes senescence and enhances chemosensitivity. *Genes Dev.* **25,** 2125–2136 (2011).
47. Hemann, M. T. *et al.* Evasion of the p53 tumour surveillance network by tumour-derived MYC mutants. *Nature* **436,** 807–811 (2005).
48. Fellmann, C. *et al.* An optimized microRNA backbone for effective single-copy RNAi. *Cell Reports* **5,** 1704–1713 (2013).
49. Chicas, A. *et al.* Dissecting the unique role of the retinoblastoma tumor suppressor during cellular senescence. *Cancer Cell* **17,** 376–387 (2010).
50. Simpson, E. M. *et al.* Genetic variation among 129 substrains and its importance for targeted mutagenesis in mice. *Nature Genet.* **16,** 19–27 (1997).
51. Navin, N. *et al.* Tumour evolution inferred by single-cell sequencing. *Nature* **472,** 90–94 (2011).
52. Baslan, T. *et al.* Genome-wide copy number analysis of single cells. *Nature Protocols* **7,** 1024–1041 (2012).
53. Baslan, T. & Hicks, J. Single cell sequencing approaches for complex biological systems. *Curr. Opin. Genet. Dev.* **26,** 59–65 (2014).
54. Folch, J., Lees, M. & Sloane Stanley, G. H. A simple method for the isolation and purification of total lipides from animal tissues. *J. Biol. Chem.* **226,** 497–509 (1957).
55. Ye, X. *et al.* Development and validation of a UPLC-MS/MS method for quantification of SKLB010, an investigational anti-inflammatory compound, and its application to pharmacokinetic studies in beagle dogs. *J. Pharm. Biomed. Anal.* **56,** 366–372 (2011).

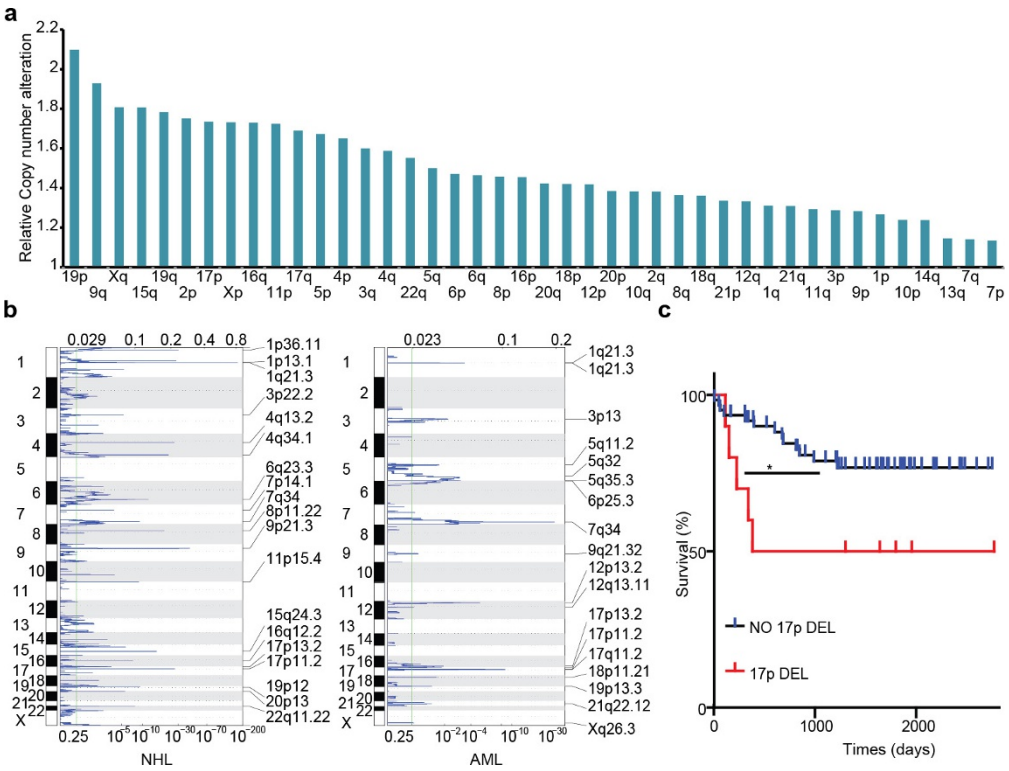

Extended Data Figure 1 | The frequency and prognostic impact of chromosome 17p deletion with the copy number loss identified by GISTIC. a, The ratio of chromosome-copy-number-altered cases within *TP53*-mutated cases compared to those within wild-type cases. *TP53* mutations were statistically correlated with 17p loss ($P < 0.001$) but also other copy number events ($P < 0.001$). **b**, Peaks of copy number loss identified by the GISTIC algorithm in NHL or AML. *x* axis, GISTIC *q* value; *y* axis, chromosome. $q < 0.25$ is considered as significant. **c**, Overall survival of human diffuse large B-cell lymphoma (DLBCL) patients with chromosome 17p deletion is significantly shortened compared to those with no 17p copy number variants, as annotated from the Gene Expression Omnibus GSE34171 series. $^*P < 0.05$ (log-rank test).

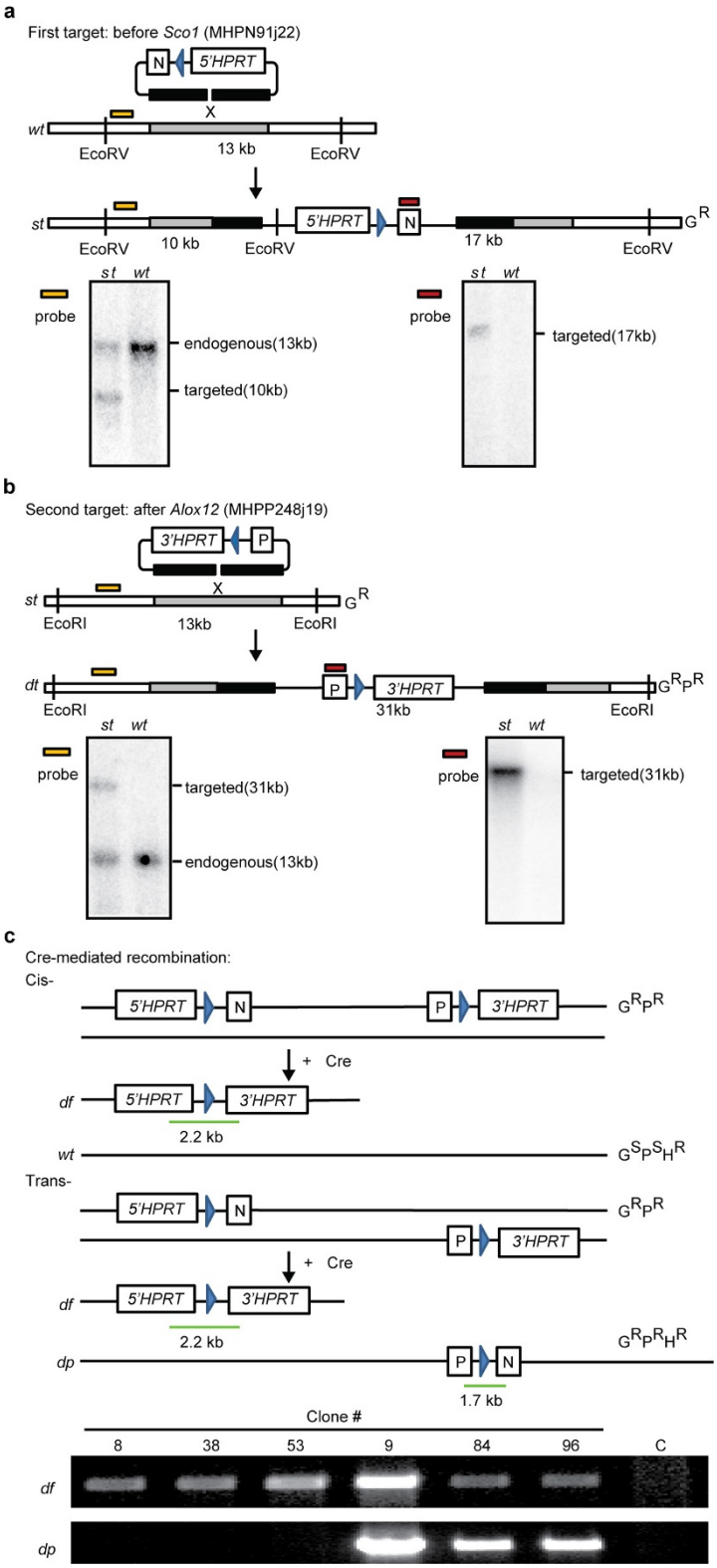

Extended Data Figure 2 | Generation of a chromosome 11B3 conditional knockout mouse. a, Top, strategy to introduce 5′ *HPRT* gene and *loxP* site telomeric to *Sco1* on chromosome 11B3 with MICER clone MHPN91j22. Bottom, Southern blot demonstrating correct targeting of the derived ES cells. *st*, single-targeted allele; *wt*, wild-type. Blue arrowheads denote *loxP* sites. **b**, Top, strategy to introduce 3′ *HPRT* gene and *loxP* site centromeric to *Alox12* on chromosome 11B3 with MICER clone MHPP248j19. Bottom, Southern blot demonstrating correct targeting of the derived ES cells. dt, double-targeted allele. **c**, Top, diagram showing the expected PCR results and drug-resistance phenotypes of doubly targeted ES cells harbouring *loxP* sites in *cis* versus in *trans*. G^R, G418 (neomycin) resistance; P^R, puromycin resistance; H^R, HAT resistance. *df*, deleted allele; *dp*, duplicated allele. Green bar indicates the PCR product location and length. Bottom, PCR results show different ES cell clones generated in **a** and **b**.

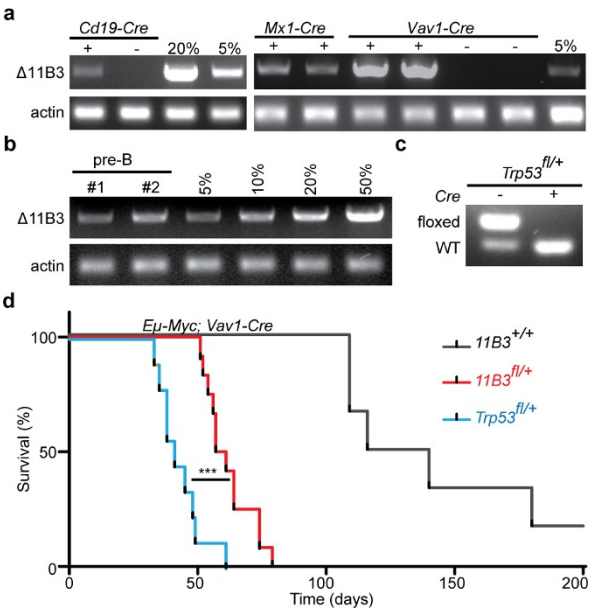

Extended Data Figure 3 | 11B3 recombination and lymphomagenesis in *Eu-Myc* model. a, The extent of 11B3 deletion in peripheral blood cells, as determined by semi-quantitative PCR, in $11B3^{fl/+}$ mice crossed to *Cd19-cre* (left), *Mx1-cre* (middle) or *Vav1-cre* (right). Genomic DNA from $11B3^{+/\Delta}$ ES cells was mixed with $11B3^{fl/+}$ cells at different ratios (5% or 20%) as a standard. For *Mx1-cre*, 6–8-week-old mice were treated with polyinosinic:polycytidylic acid (poly(I:C)) (15 mg kg^{-1} every other day, 7 times) by intraperitoneal injection. **b**, Partial 11B3 deletion in *Vav1-cre;*$11B3^{fl/+}$ pre-B cells as determined by semi-quantitative PCR, indicating incomplete recombination. **c**, Complete $Trp53^{fl/+}$ recombination in *Vav1-cre;*$Trp53^{fl/+}$ pre-B cells as determined by PCR. **d**, Tumour-free survival of *Eμ-Myc;Vav1-cre;*$Trp53^{fl/+}$ ($n = 9$), *Eμ-Myc;Vav1-cre;*$11B3^{fl/+}$ ($n = 12$) and *Eμ-Myc;Vav1-cre* ($n = 6$) mice shows that 11B3-deleted tumours have longer tumour latency than *Trp53*-loss-only controls. $^{***}P < 0.001$ (log-rank test).

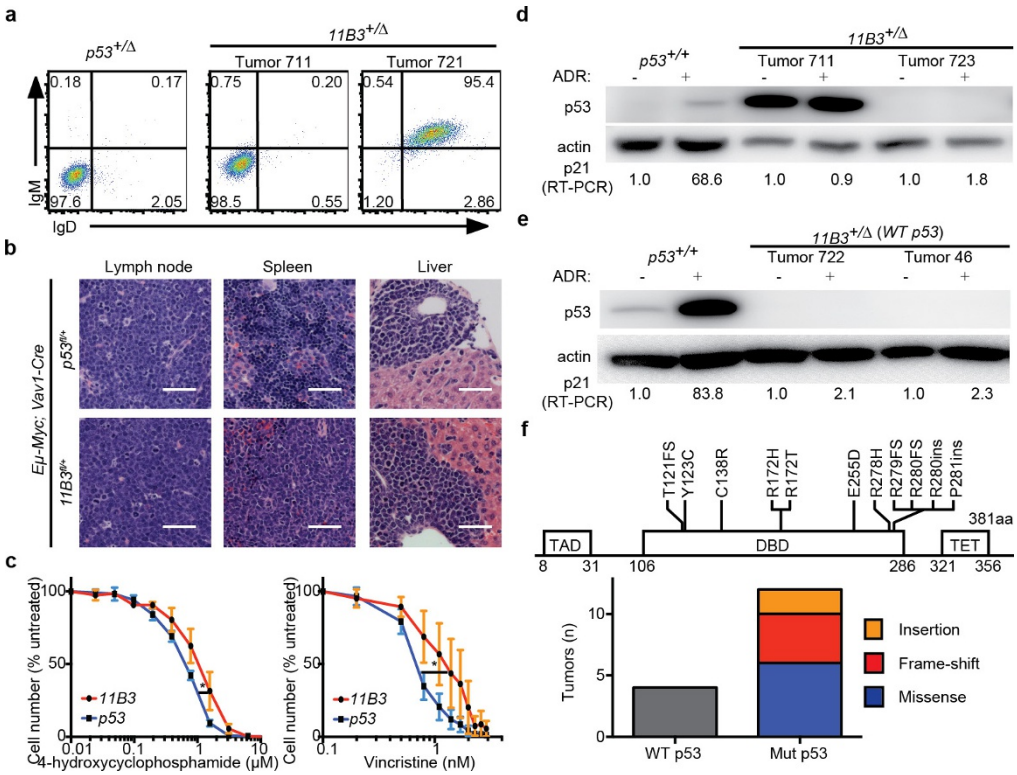

Extended Data Figure 4 | Charaterization of 11B3-deleted lymphoma. **a**, Immunophenotypes of B220$^+$ *Eμ-Myc* lymphomas generated from *Vav1-cre;p53$^{fl/+}$* or *Vav1-cre;11B3$^{fl/+}$*. 11B3-deleted lymphomas were either IgM$^-$IgD$^-$ or IgM$^+$IgD$^+$ while all the *Trp53*-null lymphomas were IgM$^-$IgD$^-$. **b**, Haematoxylin and eosin (H&E) stainings of lymph node, spleen and liver of moribund, lymphoma-bearing mice originating from *Eμ-Myc;Vav1-cre;11B3$^{fl/+}$* or *Eμ-Myc;Vav1-cre;Trp53$^{fl/+}$* genotypes. Scale bar, 50 μm. **c**, 11B3-deleted lymphoma cells isolated from enlarged lymph nodes are more resistant to chemotherapy drugs 4-hydroxycyclophosphamide (left) and vincristine (right), by *in vitro* drug sensitivity assay. Shown are representative results of three *11B3^{Δ}/Trp53^{Δframeshift}* (*11B3*) or *Trp53$^{Δ/Δ}$* (*p53*) lymphoma cell lines assayed in quadruplicate. *$P < 0.05$ (Student's two-tailed *t*-test). **d**, **e**, No functional p53 was detected in various 11B3-deleted tumours as determined by western blotting of p53 and RT–PCR analysis of *p21* induction after 4-h ADR treatment. *Eμ-Myc;Arf$^{-/-}$* (*Trp53$^{+/+}$*) lymphomas were used as a positive control and *p21* levels were normalized to untreated cells. Tumours shown in **d** were identified as missense (tumour 711) or frameshift mutations (tumour 723), while those in **e** had no detectable mutation. In total eight tumours were analysed. **f**, The scope of p53 mutations detected in chromosome 11B3-deleted lymphoma cells as determined by sequencing ($n = 12$). DBD, DNA-binding domain; FS, frameshift mutation; INS, insertion mutation; MS, missense mutation; TAD, transactivation domain; TET, tetramerization domain.

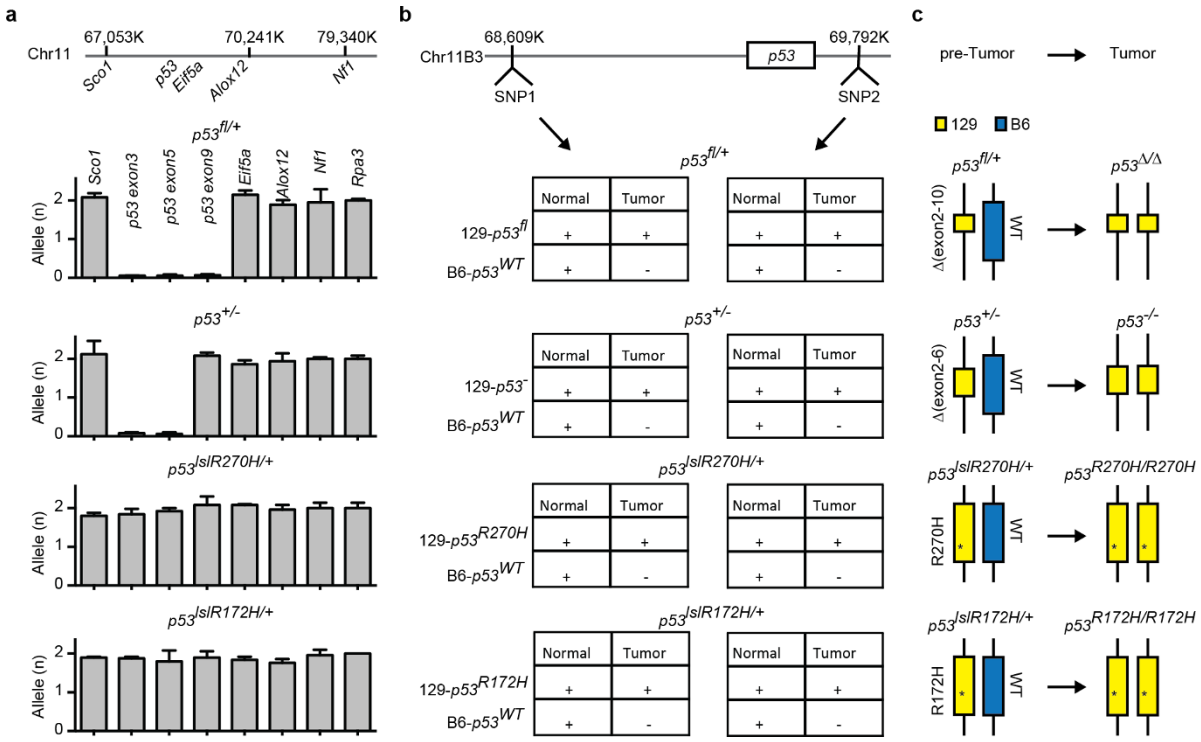

Extended Data Figure 5 | Tumours in mice heterozygous for *Trp53* mutations lose heterozygosity by duplicating the mutant *Trp53* allele. a, No chromosome 11B3 deletion was detected in various *Trp53* heterozygous mutants. Relative allele copy number of various chromosome 11B3 genes, as determined by qPCR analysis of genomic DNA from *Eμ-Myc* lymphomas derived from germline mice harbouring the following additional alleles: *Vav1-cre;Trp53*$^{fl/+}$(exon 2–10 flanked), *Trp53*$^{+/-}$ (exon 2–6 deleted), *Vav1-cre;Trp53*$^{LSL\text{-}R270H/+}$ or *Vav1-cre;Trp53*$^{LSL\text{-}R172H/+}$. *Rpa3* on chromosome 6 was used as an endogenous normalization control. **b**, SNP analysis of tumour or normal tissue (tail) genomic DNA harvested from mice in **a**, indicating that uniparental disomy occurred during *Trp53* LOH, in that C57BL/6 (B6)-derived wild-type *Trp53* allele is replaced by 129-derived *Trp53* mutant allele. Note that all *Trp53*-engineered alleles retain 129-derived SNPs; the germline wild-type *Trp53* allele is C57BL/6-derived. **c**, Cartoon summary of the results from **a** and **b**.

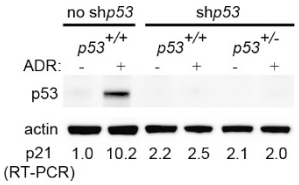

Extended Data Figure 6 | A *Trp53* shRNA induces equivalent knockdown in cells with one or two alleles of the *Trp53* gene. Pre-B cells were isolated from *Trp53*$^{+/+}$ or *Trp53*$^{+/-}$ bone marrow, and then transduced with GFP-linked *Trp53* shRNA (sh*p53*). GFP^{+} cells were sorted out by fluorescence-activated cell sorting, and treated with control wild-type pre-B cells in the present of vehicle or 1 μg ml^{-1} ADR for 4 h. p53 and *p21* levels were detected by western blotting and RT–qPCR, respectively. Shown is the representative result of three independent experiments.

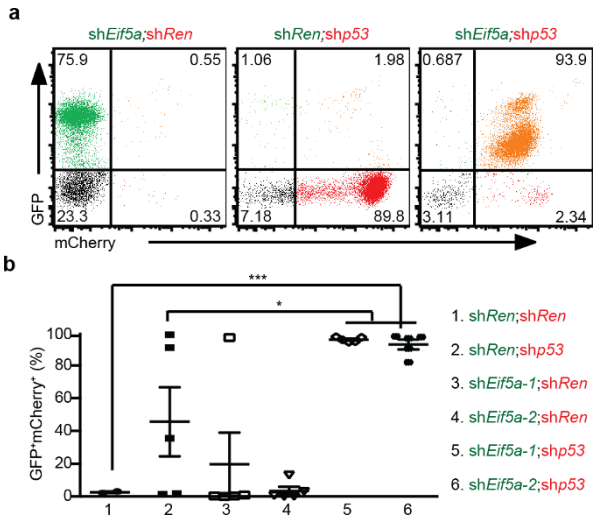

Extended Data Figure 7 | In the *Eμ-Myc* model, *Trp53* and *Eif5a* cooperate in tumorigenesis. Two-colour assay for the cooperation of *Trp53* and *Eif5a* deficiencies on lymphoma genesis. *Eμ-Myc* HSPCs retrovirally co-transduced with *GFP*- (sh*Eif5a* or sh*Ren*) and *mCherry*-linked shRNAs (sh*Ren*, sh*p53*) were transplanted into sublethally-irradiated syngeneic recipients ($n = 5$ per group). **a**, **b**, The resulting tumours were analysed by flow cytometry (**a**) and the percentage of $GFP^+mCherry^+$ lymphoma cells in each configuration was quantified (**b**). Error bars represent s.d. $^*P < 0.05$, $^{***}P < 0.001$ (two tailed *t*-test).

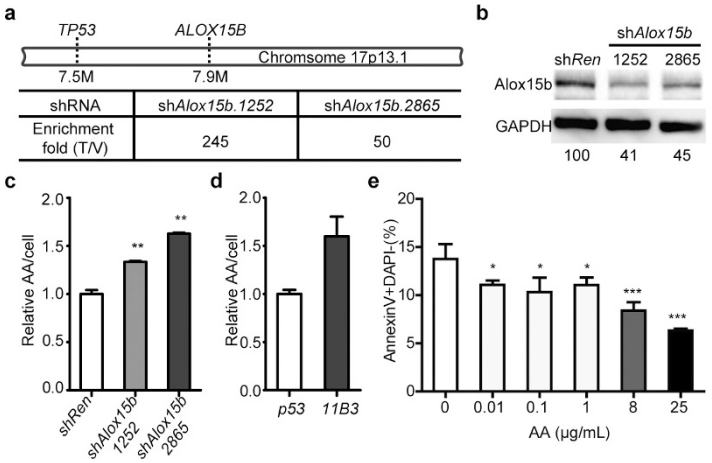

Extended Data Figure 8 | *Alox15b* deficiency promotes tumorigenesis and increases AA levels. a, Enrichment fold of sh*Alox15b.1252* and sh*Alox15b.2865* in resulting tumours (Fig. 3i, j) compared to those in initiating shRNA libraries. **b**, Knockdown efficiency of sh*Alox15b.1252* and sh*Alox15b.2865* compared to control sh*Ren* in NIH3T3 cells, as detected by western blotting and quantitated by ImageJ. **c**, Relative levels of AA per cell are increased with *Alox15b* shRNAs as measured by liquid chromatography–mass spectrometry (LC-MS). NIH3T3 cells were transduced with sh*Ren* or sh*Alox15b*. $n = 3$. $^{**}P < 0.01$ (unpaired two tailed *t*-test). **d**, Relative levels of AA per cell in $11B3^{\Delta}/Trp53^{\Delta frameshift}$ (*11B3*) lymphoma cells are higher than control cells with $Trp53^{\Delta/\Delta}$ (*p53*) as measured by LC-MS. $n = 2$. $P = 0.056$ (unpaired two tailed *t*-test). **e**, *In vitro* AA treatments reduce apoptosis, as measured by annexin V staining of pre-B cells after 20 h treatment of indicated concentration of AA. $n = 4$. $^{*}P < 0.05$; $^{***}P < 0.001$ (unpaired two tailed *t*-test).

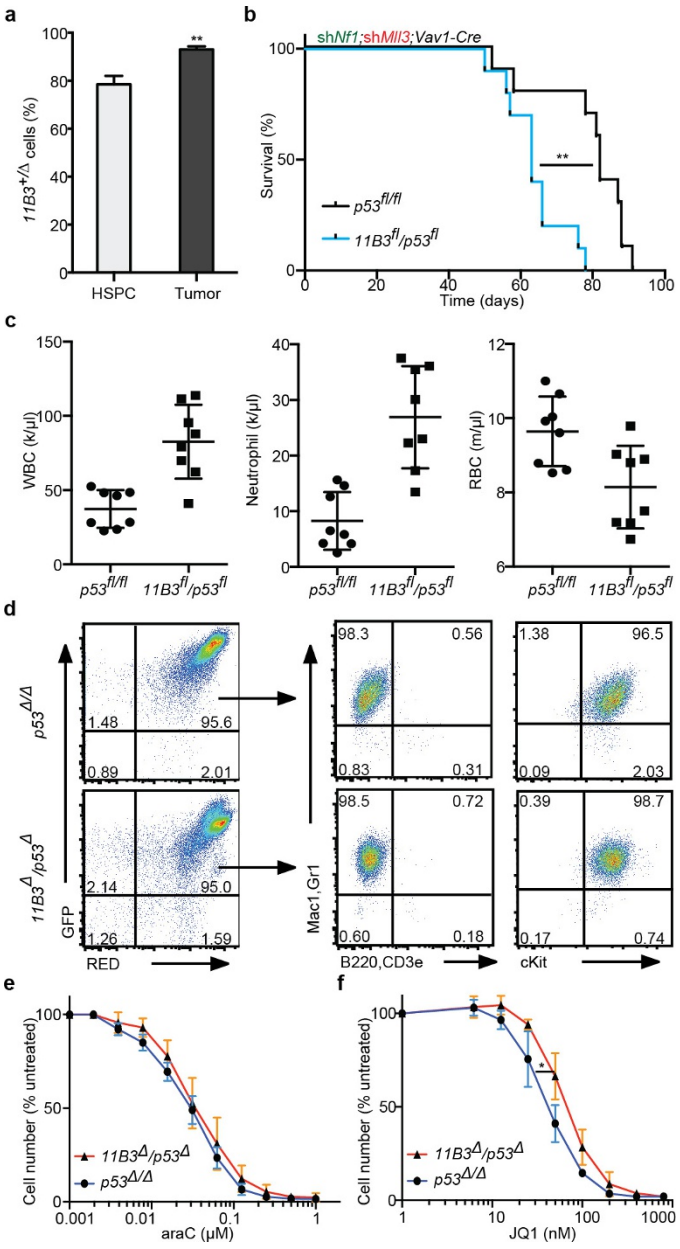

Extended Data Figure 9 | 11B3 deletion accelerates leukaemogenesis beyond *Trp53* loss alone and decreases sensitivity to the BET-protein inhibitor JQ-1. a, The percentage of 11B3 deletion as determined by qPCR in premalignant c-Kit$^+$ HSPCs ($n = 2$) and resulting leukaemia cells (tumour; $n = 4$). $^{**}P < 0.01$ (unpaired two-tailed t-test). **b**, Overall survival of recipient mice transplanted with HSPCs from *Vav1-cre;11B3^{fl}/Trp53^{fl}* or *Vav1-cre;Tr53$^{fl/fl}$* co-transduced with both *Nf1* and *Mll3* shRNAs. $^{**}P < 0.01$ (log-rank test). **c**, Complete blood cell counts of recipient mice indicate that there are more total white blood cells (WBCs) and neutrophils, and fewer red blood cells in *Vav1-cre;11B3^{fl}/Trp53^{fl}* mice compared with the *Vav1-cre;Trp53$^{fl/fl}$* control group at 8 weeks post-transplantation. (Note that two mice from each group died before analysis and were not included.) **d**, Flow cytometry analysis of GFP$^+$mCherry$^+$ leukaemic cells in the bone marrow of moribund mice in **a** shows that leukaemia cells are myeloid cells in origin and contain both sh*Nf1* and sh*Mll3*. **e, f**, *In vitro* drug sensitivity of leukaemia cells to araC (**e**) and the BET-bromodomain inhibitor JQ-1 (**f**). Shown are representative results of three *11B3$^{\Delta}$/Trp53$^{\Delta}$* and two *Trp53$^{\Delta/\Delta}$* leukaemia cell lines assayed in quadruplicate. $^{*}P < 0.05$ (Student's two-tailed t-test).

Extended Data Table 1 | Number and genotype of progeny resulting from crosses of *11B3$^{fl/+}$;Ella-cre* female mice with *Ella-cre* male mice

Progeny genotype	*11B3$^{+/\Delta}$*	*11B3$^{+/+}$*
Predicted	47	47
Observed	0*	69

No 11B3-deleted pup was produced from *11B3$^{fl/+}$* female breeders with germline *Ella-cre*, while 25 out of 94 pups were genotyped as *11B3$^{fl/+}$* without recombination.
*$P = 2.8 \times 10^{-7}$ (Chi-squared test).